1-1-2015

Universal Four-Fermion Interaction in Lattice Effective Field Theory

Kristopher Katterjohn

Universal four-fermion interaction in lattice effective field theory

By

Kristopher J. Katterjohn

A Thesis
Submitted to the Faculty of
Mississippi State University
in Partial Fulfillment of the Requirements
for the Degree of Master of Science
in Physics
in the Department of Physics and Astronomy

Mississippi State, Mississippi

August 2015

Universal four-fermion interaction in lattice effective field theory

By

Kristopher J. Katterjohn

Approved:

Gautam Rupak Lan Tai Moong
(Major Professor)

Dipangkar Dutta
(Committee Member)

R. Torsten Clay
(Committee Member)

Hendrik F. Arnoldus
(Graduate Coordinator)

R. Gregory Dunaway
Professor and Dean
College of Arts & Sciences

Name: Kristopher J. Katterjohn

Date of Degree: August 14, 2015

Institution: Mississippi State University

Major Field: Physics

Major Professor: Dr. Gautam Rupak Lan Tai Moong

Title of Study: Universal four-fermion interaction in lattice effective field theory

Pages of Study: 42

Candidate for Degree of Master of Science

In this thesis we study non-relativistic, low-energy, s-wave scattering in a four-body spin-1/2 fermion system. The scattering is caused by an attractive two-fermion contact interaction which is capable of producing a weakly bound state known as a dimer. This four-fermion system is used to study the scattering of a two-dimer system.

Using Hybrid Monte Carlo methods we compute the ground state energies of the system on a lattice. Luscher's finite-volume formula and the Effective Range Expansion are used to calculate the dimer-dimer scattering length $a_{\rm dd}$ and effective range $r_{\rm dd}$ in terms of the fermion-fermion scattering length $a_{\rm ff}$. Using these techniques we obtain the values $a_{\rm dd}/a_{\rm ff} = 0.60$ +/- 0.04 and $r_{\rm dd}/a_{\rm ff} = 3.2$ +/- 0.5. This scattering length shows excellent agreement with the numerous values in the literature. We also compare this effective range with the only currently known value in the literature.

DEDICATION

To my parents.

ACKNOWLEDGEMENTS

First, I would like to thank my thesis advisor, Dr. Gautam Rupak. He encouraged me to work independently, but he was always there to answer the many questions that I had. I could not have completed this without his help and guidance.

I would also like to thank my committee members, Dr. R. Torsten Clay and Dr. Dipangkar Dutta, for agreeing to be on my committee and for their comments and suggestions.

In addition, I would like to thank the Department of Physics and Astronomy here at Mississippi State University for accepting me into the graduate program and for financially supporting my studies through teaching assistantships. I would also like to thank the various professors with whom I have taken classes. I have learned a lot about physics during my stay here.

Most of the work in this thesis was done in collaboration with Dr. Dean Lee and Dr. Serdar Elhatisari of North Carolina State University. I have learned a lot by working with them.

Computing resources were provided by the High Performance Computing centers at Mississippi State University, North Carolina State University and RWTH Aachen University.

Partial financial support was provided by the National Science Foundation.

TABLE OF CONTENTS

LIST OF TABLES

LIST OF FIGURES

CHAPTER 1

INTRODUCTION

In this work we consider the scattering in a four-body system of spin-1/2 non-relativistic fermions interacting at low energy and producing a large scattering length. By "large" we mean that the scattering length is much larger in magnitude than the range of the interaction. We shall always work in "natural" units where $\hbar = 1 = c$.

In the low energy regime s-wave scattering provides the dominant effects [1]. This is because, at a fixed energy, higher angular momentum corresponds to a more peripheral collision. The s-wave scattering amplitude $\mathcal{A}(p)$ for non-relativistic, low-energy, two-body scattering is given by

$$\mathcal{A}(p) = \frac{2\pi}{\mu} \frac{1}{p \cot \delta_{\rm ff}(p) - ip} \,, \tag{1.1}$$

where p is the relative momentum between the fermions, μ is the effective mass of the fermions and $\delta_{\rm ff}(p)$ is the s-wave phase shift of the fermions. An analytical expansion of $p \cot \delta_{\rm ff}(p)$, known as the Effective Range Expansion (ERE), is given by [2, 3, 4, 5]

$$p \cot \delta_{\rm ff}(p) = -\frac{1}{a_{\rm ff}} + \frac{1}{2} r_{\rm ff} p^2 + O(p^4) \,, \tag{1.2}$$

where $a_{\rm ff}$ is known as the fermion-fermion scattering length and $r_{\rm ff}$ is known as the fermion-fermion effective range. Eq. (1.2) is a very general expansion that depends only on the

short-range nature of the interaction and on the analyticity of the scattering amplitude. It is common to keep only the first two terms in the right-hand side of Eq. (1.2). This is then called the "shape-independent approximation formula" [1, 6, 7] or the "effective-range theory" [8].

For scattering at sufficiently low momentum the scattering amplitude Eq. (1.1) is given by

$$\mathcal{A}(p) = \frac{2\pi}{\mu} \frac{1}{-\frac{1}{a_{\rm ff}} - ip}\,, \tag{1.3}$$

which has a pole at $p = i/a_{\rm ff}$ in the complex p plane. Then the non-relativistic energy of this state is given by

$$E_{\rm ff} = \frac{p^2}{2\mu} = \frac{-1}{2\mu a_{\rm ff}^2}\,. \tag{1.4}$$

This negative energy is expected because poles in the scattering amplitude correspond to bound states [1, 9, 10]. Here we are assuming that $|r_{\rm ff}|$ is of "natural size" or smaller. Also notice that a large scattering length yields a weakly bound state since $E_{\rm ff}$ can be made arbitrarily small in magnitude (while staying negative) for sufficiently large $|a_{\rm ff}|$. In the case of Eq. (1.4), since the complex $E_{\rm ff}$ plane is two-sheeted, we follow the usual convention of choosing the cut to lie along the positive real axis so that the first sheet is the "physical" sheet [1, 7, 9]. Then these states with $a_{\rm ff} > 0$ correspond to real bound states and states with $a_{\rm ff} < 0$ correspond to so-called virtual bound states. Henceforth, by "dimer" we shall mean a real bound state between two fermions.

There are a number of physical examples of systems which produce large scattering lengths when scattering at low energies. The scattering of neutrons and protons, which

are collectively known as nucleons, provide several examples of this. The neutron-neutron and neutron-proton scattering in the s-wave spin-singlet channel have scattering lengths of $a_{\rm nn} \sim -19$ fm [11] and $a_{\rm np} \sim -24$ fm [12], respectively. Hence, these are virtual bound states. Neutron-proton scattering in the s-wave spin-triplet channel has a scattering length of $a_{\rm np} \sim +5$ fm [13]. This real bound state is called a deuteron. In contrast, the range of these nucleon-nucleon interactions is set by the Compton wavelength of the pion, $R \sim 1/m_\pi \sim 1.4$ fm.

In 1999, George Bertsch proposed the "Many-Body X Challenge" which asks for the ground state properties of many-body systems of spin-1/2 fermions interacting with a zero-range interaction and producing an infinite scattering length (the so-called unitary limit [1]). This can be considered a somewhat idealized model of a dilute neutron matter with an attractive two-body interaction. This also leads to the concept of a unitary Fermi gas where, at low momentum, the scattering amplitude becomes

$$\mathcal{A}(p) = \frac{2\pi i}{\mu p}\,, \tag{1.5}$$

and the system is constrained by the need to conserve probability (unitarity). This limit is also important in the study of ultracold atomic gases [14], which have been experimentally realized [15, 16]. In this way, the large scattering length limit describes a universal class of phenomena that occur in atomic, nuclear and particle physics.

The four-body fermion system we will be considering is such that the two-body interaction can produce a weakly bound dimer with a scattering length $a_{\rm ff}$ that is arbitrarily large in comparison to other length scales and with an effective range $r_{\rm ff} \to 0$. This system

is completely parameterized by the two-body scattering length $a_{\rm ff}$. If the four-body system consists of a pair of weakly bound dimers, then the scattering of the dimer-dimer system is also parameterized by $a_{\rm ff}$ since it is the only available scale.

Through exact numerical calculations the dimer-dimer scattering length $a_{\rm dd}$ has been found to be $a_{\rm dd}/a_{\rm ff} = 0.60 \pm 0.01$ [17, 18]. Using a perturbative expansion around 4 spatial dimensions gives $a_{\rm dd}/a_{\rm ff} \approx 0.656$ [19]. Another estimate obtained by first calculating a complex dimer-dimer scattering length is $a_{\rm dd}/a_{\rm ff} = 0.605 \pm 0.005$ [20]. The dimer-dimer effective range $r_{\rm dd}$ seems to be much less well-known. The only currently known value is $r_{\rm dd}/a_{\rm ff} \approx 0.12$ [21].

Effective Field Theory (EFT) is a theoretical framework which takes advantage of scale separations of physical systems. It separates short-distance physics, as measured with a high-momentum scale Λ, from long-distance effects, as measured with a low-momentum scale Q. Calculations are then done using an expansion in Q/Λ. At each order of expansion, only the most general operators are used which are consistent with the symmetries of the system under investigation. This creates a model-independent framework in which to analyze the system.

The physical systems described above can be analyzed well with EFT by associating the fermion momenta p and the reciprocal of the scattering length $1/a_{\rm ff}$ with the low-momentum scale Q and the reciprocal of the range of interaction $1/R$ with high-momentum scale Λ. In a dilute many-body system we can also associate the reciprocal of the interparticle spacing with Q. Viewed in this way, $Q/\Lambda \ll 1$ and so we have a clear separation of scales.

Lattice EFT combines the theoretical ideas of EFT with numerical lattice methods. The use of a space-time lattice allows for non-perturbative calculations with tractable systematic errors introduced by known factors such as the non-zero lattice spacing and finite lattice volume. In the end, continuum results can be obtained by extrapolation.

In this work we calculate the low-energy dimer-dimer phase shift $\delta_{\rm dd}(p)$ using lattice EFT calculations and then extract the dimer-dimer scattering length $a_{\rm dd}$ and effective range $r_{\rm dd}$ in terms of $a_{\rm ff}$. We then show that the ratio $a_{\rm dd}/a_{\rm ff}$ obtained in this way shows very good agreement with the calculated values above. We also show that our effective range $r_{\rm dd}$ agrees with the sign of the cited value above, although it does not agree in magnitude.

CHAPTER 2

FORMALISM

2.1 Continuum Theory

We begin with a description of the two-fermion interaction in the continuum. As stated in Chapter 1, we are focusing on s-wave interactions. Concentrating on the dominant interaction of interest, which can yield a weakly bound dimer, the two-body interaction must be in the spin (or isospin, where applicable) anti-symmetric channel. This is obviously true if the fermions are identical, due to the Pauli exclusion principle. This can also be seen to be true in the case of the deuteron-forming neutron-proton interaction: here the scattering is in the spin symmetric, isospin anti-symmetric channel.

We only work in the non-relativistic regime, so the theory must be Galilean invariant. So, in the Lagrangian density $\mathcal{L}$ describing this system, this gives a kinetic term of

$$\psi^\dagger [i\partial_t + \frac{\nabla^2}{2m}]\psi \,, \tag{2.1}$$

where ψ represents a two-component fermion field $\binom{\psi_\uparrow}{\psi_\downarrow}$, and m is the fermion mass. Since we deal only with fermions, the wavefunction must be anti-symmetric. This gives an interaction term of

$$-\frac{g}{4}(\psi\sigma_2\psi)^\dagger(\psi\sigma_2\psi) \,, \tag{2.2}$$

where the Pauli matrix σ_2 acts only on the spin (or isospin) components of ψ, and g is a coupling which can be tuned to reproduce either a particular fermion-fermion scattering length a_{ff} or a particular fermion-fermion binding energy B. It can be shown, using a "power counting" argument [22, 23], that further terms include derivatives and these are suppressed in the Q/Λ expansion. Therefore, our two-fermion interaction is described by the Lagrangian density

$$\begin{aligned}\mathcal{L}[\psi] =&\psi^\dagger[i\partial_t + \frac{\nabla^2}{2m}]\psi - \frac{g}{4}(\psi\sigma_2\psi)^\dagger(\psi\sigma_2\psi) \\ =&\psi^\dagger[i\partial_t + \frac{\nabla^2}{2m}]\psi - g(\psi^\dagger_\uparrow\psi_\uparrow)(\psi^\dagger_\downarrow\psi_\downarrow)\,.\end{aligned} \tag{2.3}$$

With these definitions, the action and partition function are given by

$$S[\psi] = \int\!\!\!\int\!\!\!\int\!\!\!\int d^4x\,\mathcal{L}[\psi] \tag{2.4}$$

and

$$\mathcal{Z} = \int\!\!\!\int\!\!\!\int\!\!\!\int \mathcal{D}\psi\, e^{iS[\psi]}\,, \tag{2.5}$$

respectively, where the partition function $\mathcal{Z}$ is expressed as a functional integral over the fields ψ [24].

Our system consists of four fermions subject to the two-body interaction described above. One approach to solving the four-body problem is using the Faddeev-Yakubovsky equations [25]; however, this is generally not an easy task [26, 27]. The rest of this chapter is dedicated to obtaining a theory for numerically solving for the ground state properties of the system, which plays an important role in describing the dimer-dimer scattering considered later.

2.2 Euclidean Time Projection

We rewrite the equations in Section 2.1 for use in numerical lattice calculations by introducing the so-called Euclidean time variable $\tau = it$. This is known as a Wick rotation [28]. The Euclidean Lagrangian and Euclidean action are then defined to be

$$\mathcal{L}_E[\psi] = \psi^\dagger[\partial_\tau - \frac{\nabla^2}{2m}]\psi + g(\psi_\uparrow^\dagger\psi_\uparrow)(\psi_\downarrow^\dagger\psi_\downarrow) \tag{2.6}$$

and

$$S_E[\psi] = \iint\!\!\!\!\iint d^4x_E\, \mathcal{L}_E[\psi]\,, \tag{2.7}$$

respectively, where $d^4x_E = id^4x$. With these definitions the partition function becomes

$$\mathcal{Z}_E = \iint\!\!\!\!\iint \mathcal{D}\psi\, e^{-S_E[\psi]}\,. \tag{2.8}$$

Using Euclidean time is useful when considering large τ [29]. Let $\mathcal{H}$ be the Hamiltonian for some quantum system with a non-degenerate ground state. Label the eigenstates and energies of $\mathcal{H}$ as

$$\mathcal{H}\,|\phi_n\rangle = E_n\,|\phi_n\rangle\ , \tag{2.9}$$

$$E_0 < E_1 \leq E_2 \leq \cdots\,. \tag{2.10}$$

Now consider decaying exponentials of $\mathcal{H}$:

$$e^{-\mathcal{H}\tau}\,|\phi_n\rangle = e^{-E_n\tau}\,|\phi_n\rangle\ . \tag{2.11}$$

Then for states $|\psi\rangle$ with $\langle\phi_0|\psi\rangle \neq 0$ we have

$$\begin{aligned} e^{-\mathcal{H}\tau}|\psi\rangle =& e^{-\mathcal{H}\tau}\sum_n \Big(|\phi_n\rangle \langle\phi_n|\psi\rangle \\ =& \sum_n \Big(e^{-E_n\tau}|\phi_n\rangle \langle\phi_n|\psi\rangle \\ \to& e^{-E_0\tau}|\phi_0\rangle \langle\phi_0|\psi\rangle \end{aligned} \tag{2.12}$$

as $\tau \to \infty$. In this way using Euclidean time projection allows us to extract information about the ground state of the Hamiltonian.

2.3 Lattice Theory

The lattice theory is obtained by discretizing space-time. An important property of the lattice theory is that there are only finite degrees of freedom, given by the spatial and temporal lattice sites. In the continuum theory there are infinite degrees of freedom, so numerically calculating arbitrary partition functions becomes impracticable.

We use a cubic periodic lattice consisting of L^3 spatial lattice sites and L_t temporal lattice sites. The spatial and temporal lattice spacings are denoted by b and b_t, respectively. The lattice space-time coordinates are denoted by $(\vec{n}, n_t)$, where $\vec{n}$ is a three-dimensional integer vector labelling the spatial lattice sites and n_t is an integer labelling the lattice steps in the temporal direction. The lattice spatial unit vectors are denoted by $\hat{l} = \hat{1}, \hat{2}, \hat{3}$.

The lattice action is obtained by discretizing the Euclidean action in Eq. (2.7):

$$
\begin{aligned}
S_E[\psi] = &\int\!\!\int d^4x_E\, \mathcal{L}_E[\psi] \\
\to &b^3 b_t \sum_{\vec{n},n_t,i=\uparrow\downarrow} \psi_i^\dagger(\vec{n},n_t)\frac{\psi_i(\vec{n},n_t+1)-\psi_i(\vec{n},n_t)}{b_t} \\
&- b^3 b_t \sum_{\vec{n},n_t,i=\uparrow\downarrow}\sum_{l=1,2,3} \psi_i^\dagger(\vec{n},n_t)\frac{\psi_i(\vec{n}+\hat{l},n_t)+\psi_i(\vec{n}-\hat{l},n_t)-2\psi_i(\vec{n},n_t)}{2mb^2} \\
&+ b^3 b_t \sum_{\vec{n},n_t} g(\psi_\uparrow^\dagger(\vec{n},n_t)\psi_\uparrow(\vec{n},n_t))(\psi_\downarrow^\dagger(\vec{n},n_t)\psi_\downarrow(\vec{n},n_t)).
\end{aligned}
\tag{2.13}
$$

It is convenient to use physical quantities expressed in lattice units of b. These are denoted with a "hat" and are given by

$$\hat{m} = bm\,, \tag{2.14}$$

$$\hat{\psi}(\vec{n},n_t) = b^{\frac{3}{2}}\psi(\vec{n},n_t)\,, \tag{2.15}$$

$$\hat{g} = \frac{g}{b^2}\,. \tag{2.16}$$

We also define

$$\alpha_t = \frac{b_t}{b}\,, \tag{2.17}$$

$$h = \frac{\alpha_t}{2\hat{m}}\,. \tag{2.18}$$

With these definitions the lattice action may be written more simply as

$$
\begin{aligned}
S_E[\psi] = &\sum_{\vec{n},n_t,i=\uparrow\downarrow} \hat{\psi}_i^\dagger(\vec{n},n_t)[\hat{\psi}_i(\vec{n},n_t+1)-(1-6h)\hat{\psi}_i(\vec{n},n_t)] \\
&- h\sum_{\vec{n},n_t,i=\uparrow\downarrow}\sum_{l=1,2,3} \hat{\psi}_i^\dagger(\vec{n},n_t)[\hat{\psi}_i(\vec{n}+\hat{l},n_t)+\hat{\psi}_i(\vec{n}-\hat{l},n_t)] \\
&+ \hat{g}\alpha_t \sum_{\vec{n},n_t} (\hat{\psi}_\uparrow^\dagger(\vec{n},n_t)\hat{\psi}_\uparrow(\vec{n},n_t))(\hat{\psi}_\downarrow^\dagger(\vec{n},n_t)\hat{\psi}_\downarrow(\vec{n},n_t))\,.
\end{aligned}
\tag{2.19}
$$

The lattice partition function is calculated by introducing complex anti-commuting Grassmann [24] fields c, c^* defined on the lattice coordinates:

$$\mathcal{Z}_E(L_t) = \int [\prod_{\vec{n},n_t,i=\uparrow\downarrow} dc_i(\vec{n},n_t) dc_i^*(\vec{n},n_t)] \, e^{-S_E(c,c^*)} \,, \tag{2.20}$$

$$S_E(c,c^*) = S_E^{\text{free}}(c,c^*) + \hat{g}\alpha_t \sum_{\vec{n},n_t} [c_\uparrow^*(\vec{n},n_t) c_\uparrow(\vec{n},n_t)][c_\downarrow^*(\vec{n},n_t) c_\downarrow(\vec{n},n_t)] \,, \tag{2.21}$$

$$\begin{aligned} S_E^{\text{free}}(c,c^*) = & \sum_{\vec{n},n_t,i=\uparrow\downarrow} c_i^*(\vec{n},n_t)[c_i(\vec{n},n_t+1) - (1-6h)c_i(\vec{n},n_t)] \\ & - h \sum_{\vec{n},n_t,i=\uparrow\downarrow} \sum_{l=1,2,3} c_i^*(\vec{n},n_t)[c_i(\vec{n}+\hat{l},n_t) + c_i(\vec{n}-\hat{l},n_t)] \,. \end{aligned} \tag{2.22}$$

These Grassmann fields are defined to satisfy periodic boundary conditions for the spatial coordinates,

$$c_i(\vec{n}+L\hat{1},n_t) = c_i(\vec{n}+L\hat{2},n_t) = c_i(\vec{n}+L\hat{3},n_t) = c_i(\vec{n},n_t) \,, \tag{2.23}$$

$$c_i^*(\vec{n}+L\hat{1},n_t) = c_i^*(\vec{n}+L\hat{2},n_t) = c_i^*(\vec{n}+L\hat{3},n_t) = c_i^*(\vec{n},n_t) \,, \tag{2.24}$$

and anti-periodic boundary conditions for the temporal coordinates,

$$c_i(\vec{n},n_t+L_t) = -\, c_i(\vec{n},n_t) \,, \tag{2.25}$$

$$c_i^*(\vec{n},n_t+L_t) = -\, c_i^*(\vec{n},n_t) \,. \tag{2.26}$$

The lattice partition function $\mathcal{Z}_E$ and action $S_E(c,c^*)$ may be rewritten using an auxiliary field [30] as

$$\mathcal{Z}_E(L_t) = \prod_{\vec{n},n_t,i=\uparrow\downarrow} \left[\frac{1}{2\pi} \int_{-\pi}^{\pi} ds(\vec{n},n_t)\right] \int dc_i(\vec{n},n_t) dc_i^*(\vec{n},n_t) \, e^{-S_E^{\text{aux}}(c,c^*,s)} \,, \tag{2.27}$$

$$S_E^{\text{aux}}(c,c^*,s) = S_E^{\text{free}}(c,c^*) - \sqrt{-\hat{g}\alpha_t} \sum_{\vec{n},n_t} \sin[s(\vec{n},n_t)]\rho(\vec{n},n_t) \,, \tag{2.28}$$

where the total number density $\rho(\vec{n}, n_t) = \rho_\downarrow(\vec{n}, n_t) + \rho_\uparrow(\vec{n}, n_t)$ with the spin-up and spin-down densities written as $\rho_\uparrow(\vec{n}, n_t) = c^*_\uparrow(\vec{n}, n_t)c_\uparrow(\vec{n}, n_t)$ and $\rho_\downarrow(\vec{n}, n_t) = c^*_\downarrow(\vec{n}, n_t)c_\downarrow(\vec{n}, n_t)$, respectively. The rewriting of the lattice action using an auxiliary field is analogous to the Hubbard-Stratonovich Transformation [31, 32] given by

$$e^{\frac{1}{4a}x^2} = \sqrt{\frac{a}{\pi}} \int_{-\infty}^{\infty} e^{-au^2 - xu}\, du\,, \tag{2.29}$$

for $a > 0$. The advantage of introducing the auxiliary field is that the interaction is now linear in the number density and the spin-up and spin-down particles decouple.

We may further rewrite the lattice action using the correspondence [33]

$$\begin{aligned} \mathrm{Tr}[:\, f_{L_t-1}(a^\dagger(\vec{n}), a(\vec{n})) : \times \cdots \times : f_0(a^\dagger(\vec{n}), a(\vec{n}))\, :] = \\ \int \Big[\prod_{n_t=0}^{L_t-1} dc^*(\vec{n}, n_t) dc(\vec{n}, n_t)\Big] \Big(\\ e^{c^*(\vec{n},0)(c(\vec{n},0)+c(\vec{n},L_t-1))} e^{c^*(\vec{n},1)(c(\vec{n},1)-c(\vec{n},0))} \cdots e^{c^*(\vec{n},L_t-1)(c(\vec{n},L_t-1)-c(\vec{n},L_t-2))} \\ \Big[\prod_{n_t=0}^{L_t-1} f_{n_t}(c^*(\vec{n}, n_t), c(\vec{n}, n_t))\Big] \Big(\end{aligned} \tag{2.30}$$

where $a^\dagger$ and a denote the usual creation and annihilation operators, respectively. The anti-periodicity in time of the Grassmann fields appears in Eq. (2.30). We now define the transfer matrix operators M by

$$M(s, n_t) = :\exp \quad -\alpha_t H_{\text{free}} + \sqrt{-\hat{g}\alpha_t} \sum_{\vec{n}} \Big(\sin[s(\vec{n}, n_t)] \rho^{a^\dagger a}(\vec{n}) \Big) \Big(:, \tag{2.31}$$

where the free lattice Hamiltonian H_{free} is defined on the spatial lattice sites using the creation and annihilation operators:

$$H_{\text{free}} = \frac{1}{2\hat{m}} \sum_{\vec{n}, i=\uparrow\downarrow} \sum_{l=1,2,3} \Big(a_i^\dagger(\vec{n}) [a_i(\vec{n} + \hat{l}) + a_i(\vec{n} - \hat{l}) - 2a_i(\vec{n})]\,. \tag{2.32}$$

The transfer matrix operators represent time evolution by discrete steps of length α_t, analogous to e^{-iHt} in the continuum theory. The form of the auxiliary field in Eq. (2.27) was chosen because it reduces the large fluctuations in the transfer matrix elements when compared to other auxiliary fields [30]. The : symbols in Eq. (2.30) and Eq. (2.31) indicate "normal ordering" where all of the creation operators are moved to the left of the annihilation operators in products. Now the partition function may be written as

$$\mathcal{Z}_E(L_t) = \prod_{\vec{n},n_t} \left[\left(\frac{1}{2\pi} \int_{-\pi}^{\pi} ds(\vec{n},n_t) \right] \mathrm{Tr}[M(s,L_t-1)\cdots M(s,0)] \right. . \tag{2.33}$$

In comparison to Eq. (2.31), the transfer matrix without auxiliary fields is given by

$$\hat{M} = : \exp \quad -\alpha_t H_{\mathrm{free}} - \hat{g}\alpha_t \sum_{\vec{n}} \left(\rho_{\uparrow}^{a^\dagger a}(\vec{n}) \rho_{\downarrow}^{a^\dagger a}(\vec{n}) \right) : \ . \tag{2.34}$$

This is used later to provide exact numerical lattice values where computationally feasible.

In the lattice calculations, the partition function is evaluated with two spin-up and two spin-down fermions with zero total center-of-mass momentum. The partition function can then be expressed in terms of the square of a determinant involving two fermions [34],

$$\mathcal{Z}_E(L_t) = \prod_{\vec{n},n_t} \left[\left(\frac{1}{2\pi} \int_{-\pi}^{\pi} ds(\vec{n},n_t) \right] \left[\det \mathbf{M}(s(\vec{n},n_t),L_t) \right]^2 \right. , \tag{2.35}$$

where

$$[\mathbf{M}(s,L_t)]_{\vec{p}',\vec{p}} = \langle \vec{p}' | \, M(s,L_t-1)\cdots M(s,0) \, | \vec{p} \rangle \ , \tag{2.36}$$

for single-fermion states $|\vec{p}\rangle$ and $|\vec{p}'\rangle$ with momenta $\vec{p}$ and $\vec{p}'$, respectively. The determinant is squared because in the transfer matrix formalism with an auxiliary field the determinant for spin-up fermions is equal to the determinant for spin-down fermions. When perform-

ing the calculations we only use two spin-up fermions and then square the corresponding determinant for the partition function in Eq. (2.35).

There is a well-known numerical "sign problem" that exists in many systems of interacting fermions [35, 36]. There is no general solution to the sign problem, but there are some workarounds for some systems. In Eq. (2.36), the $\mathbf{M}$ matrix elements are all real, so $\det \mathbf{M}$ is also real. This implies that $[\det \mathbf{M}]^2$ is non-negative, so there is no sign problem present in the partition function in Eq. (2.35).

Consider the classical partition function of a system with a countable number of states q:

$$\mathcal{Z}_c(\beta) = \sum_q e^{-\beta E(q)} \,. \tag{2.37}$$

Then for small $\delta\beta$

$$\begin{aligned} \frac{\mathcal{Z}_c(\beta)}{\mathcal{Z}_c(\beta - \delta\beta)} =& \frac{\sum_q e^{-\beta E(q)}}{\sum_q e^{-(\beta-\delta\beta)E(q)}} \\ \to& \frac{e^{-\beta E_{c,0}}}{e^{-(\beta-\delta\beta)E_{c,0}}} \\ =& e^{-E_{c,0}\delta\beta} \end{aligned} \tag{2.38}$$

as $\beta \to \infty$, where $E_{c,0}$ is the ground state energy of this system. In analogy to this we define the energy of the dimer-dimer system as a function of Euclidean time to be

$$E(t) = -\frac{1}{\alpha_t} \log \frac{\mathcal{Z}_E(L_t)}{\mathcal{Z}_E(L_t - 1)} \,, \tag{2.39}$$

where $t = \alpha_t L_t$. Another derivation of Eq. (2.39), again reminiscent of thermal physics, is to define $E(t) = -\frac{\partial}{\partial t} \log \mathcal{Z}_E(t)$ and then discretize the time derivative.

For large L_t, the ground state energy of the dimer-dimer system is the primary contributor to Eq. (2.39). This ground state energy E_0 is given by

$$e^{-\alpha_t E_0} = \lim_{L_t \to \infty} \frac{\mathcal{Z}_E(L_t)}{\mathcal{Z}_E(L_t - 1)} \,. \tag{2.40}$$

A Hybrid Monte Carlo process—described in detail in Section 3.3—is used to calculate the ground state energy of the system. Using this ground state energy, the low-momentum scattering phase shift for the dimer-dimer system can be calculated using Lüscher's formula as explained in Section 3.2.

CHAPTER 3

FINITE-VOLUME AND LATTICE METHODS

3.1 Tuning the Lattice Coupling

We tune the lattice coupling $\hat{g}$ discussed in Section 2.3 to reproduce different two-body binding energies. These binding energies correspond to poles in the fermion-fermion scattering amplitude which is calculated by summing the Feynman diagrams in Figure 3.1[1]. Given that our contact interaction is momentum-independent, no momentum flows from one bubble to another and so the sum becomes a geometric series. Then the coupling $\hat{g}$ is related to the location of the energy pole $E_{\text{pole}} = \frac{p^2}{m}$ by the relation [37, 38, 39]

$$-\frac{1}{\hat{g}\alpha_t} = \lim_{L\to\infty} \frac{1}{L^3} \sum_{\vec{n}} \left(\frac{1}{\exp(-E_{\text{pole}}\alpha_t) - 1 + 2\alpha_t\omega(2\pi\vec{n}/L) - \alpha_t^2\omega^2(2\pi\vec{n}/L)} \right), \tag{3.1}$$

where

$$\omega(\vec{p}) = \frac{1}{\hat{m}} \sum_{i=1}^{3} \left(1 - \cos p_i \right) \tag{3.2}$$

is the dispersion relation on the lattice. The coupling $\hat{g}$ is tuned to give the desired binding energies $B^{(\infty)} = -E_{\text{pole}}$ in a large box of length $L \geq 50$.

[1] This figure is taken from Ref. [39].

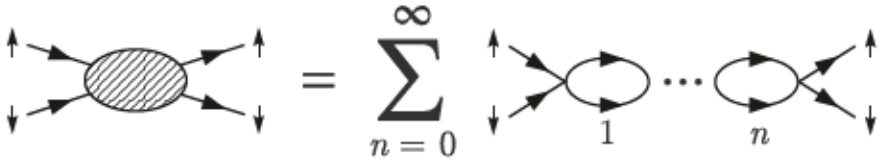

Figure 3.1

Feynman diagrams for fermion-fermion scattering

3.2 Lüscher's Formula and Phase Shifts

3.2.1 Lüscher's Formula

In a periodic box the energy levels of a two-body system are discrete regardless of an interaction. When an interaction exists between the two particles, the energy levels are simply shifted relative to the free energy spectrum. Lüscher's finite-volume formula [40, 41] relates these energy levels to the infinite-volume, continuum scattering phase shifts, δ. Assuming the two-body system has zero total linear momentum, the infinite-volume two-body phase shifts of the system in a periodic box of length L are related to the finite-volume relative momentum of the two particles, p, by the relation

$$p \cot \delta(p) = \frac{1}{\pi L} S(\eta) \,, \tag{3.3}$$

where $\eta = (\frac{pL}{2\pi})^2$ and the regulated three-dimensional zeta function is given by

$$S(\eta) = \lim_{\Lambda \to \infty} \left[\sum_{\vec{n}} \left(\frac{\Theta(\Lambda^2 - \vec{n}^2)}{\vec{n}^2 - \eta} - 4\pi\Lambda \right] \right(\tag{3.4}$$

3.2.2 Fermion-fermion Scattering Lengths on the Lattice

As described later, we rescale the dimer-dimer scattering parameters by the fermion-fermion scattering length. In the infinite-volume and continuum limits the fermion-fermion binding energy for a zero-range interaction is given by $B^{(\infty)} = 1/(ma_{\rm ff}^2)$. In order to minimize lattice artifacts we compute the fermion-fermion scattering length on the lattice.

We start by fixing a particular $B^{(\infty)}$. Then, using exact transfer matrix calculations (without auxiliary fields), we calculate the lowest s-wave fermion-fermion scattering energies on a variety of lattice sizes, L. For each L, this energy $E_{\rm ff}$ is related to the relative momenta of the fermions p simply by

$$E_{\rm ff} = \frac{p^2}{m}\,. \tag{3.5}$$

With this p we can obtain $p\cot\delta_{\rm ff}(p)$ by using Eq. (3.3) for each L. Notice that, since we are using the lowest scattering energy, p decreases as L increases. We then fit the $\big(p, p\cot\delta_{\rm ff}(p)\big)$ data using the truncated ERE,

$$p\cot\delta_{\rm ff}(p) = -\frac{1}{a_{\rm ff}^{\rm latt}} + \frac{1}{2}r_{\rm ff}^{\rm latt}p^2 + \frac{1}{2}s_{\rm ff}^{\rm latt}p^4\,. \tag{3.6}$$

Thus we obtain the scattering length $a_{\rm ff}^{\rm latt}$ on the lattice.

Table 3.1 shows several fermion-fermion binding energies and the corresponding fermion-fermion continuum and lattice scattering lengths. Notice that the ratio $a_{\rm ff}^{\rm latt}/a_{\rm ff}$ increases as $B^{(\infty)}$ increases. This is because larger binding energies correspond to more tightly bound states and these states are more sensitive to the effects of the non-zero lattice spacing.

Table 3.1

Continuum and lattice fermion-fermion scattering lengths

$B^{(\infty)}$ (MeV)	$a_{\rm ff}$ (fm)	$a_{\rm ff}^{\rm latt}$ (fm)	$a_{\rm ff}^{\rm latt}/a_{\rm ff}$
2.2246	4.31752	4.37635	1.01363
3.0	3.71792	3.78163	1.01714
3.5	3.44212	3.50865	1.01933
5.0	2.87989	2.95386	1.02569

3.2.3 Dimer-dimer Momenta and Phase Shifts

For infinite-volume, continuum dimer-dimer scattering, the relative momentum p of the dimers is related to the dimer-dimer energy $E_{\rm dd}^{(\infty)}$ by

$$E_{\rm dd}^{(\infty)}(p) = \frac{p^2}{2\mu^{(\infty)}} - 2B^{(\infty)}\,, \tag{3.7}$$

where $\mu^{(\infty)}$ is the continuum two-dimer reduced mass and $B^{(\infty)}$ is the infinite-volume dimer binding energy. Eq. (3.7) must be modified to describe the relationship between the energy and momentum in a finite-volume, discrete lattice. For non-zero lattice spacing the dimer mass gets renormalized from its continuum value $\mu^{(\infty)} = m_{\rm d}/2$, where $m_{\rm d} = 2m$ is the dimer mass. This lattice effective dimer mass $\mu^{(L)}$ is calculated numerically using the dimer dispersion relation in a large box $L = 50$, in order to minimize the finite-volume effects. The finite-volume lattice binding energy $B^{(L)}$, which differs from $B^{(\infty)}$, is calculated using exact transfer matrix calculations (without auxiliary fields). A finite-volume topological factor $\tau_{\rm d}^{(L)}(\eta)$ is also needed to account for the wrapping of the dimer wavefunction around the periodic boundary [42, 43, 44].

The numerical lattice calculations described in Chapter 2 and Section 3.3 are used to determine the finite-volume energies of the four-body system, $E_{\mathrm{dd}}^{(L)}$. The finite-volume relative momentum of the two-dimer system is related to the finite-volume four-body energies and dimer binding energies by

$$E_{\mathrm{dd}}^{(L)}(p) = \frac{p^2}{2\mu^{(L)}} - 2B^{(\infty)} + 2\tau_{\mathrm{d}}^{(L)}(\eta)\Delta E_{\mathrm{d}}^{(L)}\,, \tag{3.8}$$

where $\Delta E_{\mathrm{d}}^{(L)} = B^{(\infty)} - B^{(L)}$ is the finite-volume bound-state energy shift in the two-body center-of-mass frame. In the $L \to \infty$ limit, $\tau_{\mathrm{d}}^{(L)}(\eta) \to 1$ and $\Delta E_{\mathrm{d}}^{(L)} \to 0$, and we obtain Eq. (3.7). The topological volume factor $\tau_{\mathrm{d}}^{(L)}$ for the s-wave dimer wavefunction wrapping around the periodic boundary a single time is given by [45]

$$\tau_{\mathrm{d}}^{(L)}(\eta) = \frac{1}{\mathcal{N}(\eta)} \sum_{\vec{k}} \left(\frac{\frac{1}{3}\sum_{i=1}^{3}\cos(k_i L/2)}{(\vec{k}^2 - \eta^2)^2}, \right. \tag{3.9}$$

$$\mathcal{N}(\eta) = \sum_{\vec{k}} \left(\frac{1}{(\vec{k}^2 - \eta^2)^2}\,, \right. \tag{3.10}$$

where $\vec{k}$ are integer vectors and $\vec{k}^2 \neq \eta^2$.

Given the lattice energies $E_{\mathrm{dd}}^{(L)}$ and $B^{(L)}$, the finite-volume two-dimer relative momentum p is the one satisfying Eq. (3.8). This p is determined iteratively by beginning with $\tau_{\mathrm{d}}^{(L)}(\eta) = 1$ and then recursively solving for p^2 and $\tau_{\mathrm{d}}^{(L)}(\eta)$ using Eq. (3.8) and Eq. (3.9) until they converge. Using this p^2 (which corresponds to a particular η), Eq. (3.4) is used directly to calculate the left-hand side of Eq. (3.3).

3.3 Hybrid Monte Carlo and Importance Sampling

3.3.1 Markov Chain Monte Carlo

Consider a system which can be in a countable number of states $s_1, s_2, \cdots$. At time $t = 0$ the state of the system is given by $\chi(0)$ and at subsequent time steps $t = 1, 2, \cdots$ the system changes its state randomly to states given by $\chi(1), \chi(2), \cdots$. This system has the property that if at time t the system is in the some state s_i, $\chi(t) = s_i$, then the probability that the system transitions to state s_j at time $t + 1$, $\chi(t + 1) = s_j$, does not depend on any time prior to t. In addition, the probabilities for the system to change from one particular state to another does not depend on the time t. This is known as a Markov chain [46, 47].

Monte Carlo methods are algorithms which use random numbers to model processes which are often too difficult or computationally intractable to be analyzed otherwise [48, 49]. Monte Carlo methods have wide-ranging applications, but most often they have been used to estimate the value of multiple integrals over a large number of dimensions [50]. Often times the contributions to the value we want to estimate from different regions of the sample space vary strongly. One important technique, called Importance Sampling, is often used to improve the accuracy of the simulations by concentrating on regions of the sample space which are most "important" for estimating the desired value [47, 48, 50]. This is done is such a way so that the result is still unbiased.

Markov Chain Monte Carlo (MCMC) methods are Monte Carlo methods where the random samples are drawn using a specially constructed Markov Chain. The Metropolis-Hastings algorithm [51, 52] is a very popular method for implementing MCMC with Importance Sampling. This algorithm is built-in to the algorithm discussed in 3.3.3.

3.3.2 Hybrid Monte Carlo

Hybrid Monte Carlo (HMC)—also known as Hamiltonian Monte Carlo—is a type of MCMC in which the new, proposed states are generated by computing trajectories according to space-time discretized Hamiltonian dynamics. The variables of interest are regarded as the generalized coordinates in Hamilton's equations of motion. Generalized momenta are then introduced, typically generated randomly according to a Gaussian distribution, in order to propagate forward in "time." Hamiltonian dynamics have several properties, such as time-reversibility and preservation of volume, which simplify both the analysis and implementation of MCMC updates [53].

As mentioned briefly in Chapter 2, HMC simulations are used to calculate $\frac{\mathcal{Z}_E(L_t)}{\mathcal{Z}_E(L_t-1)}$ in order to determine the ground state energy of the dimer-dimer system. In this HMC scheme the variables of interest are auxiliary field configurations $s(\vec{n}, n_t)$, so there are $L^3 \times L_t$ "generalized coordinates" in Hamilton's equations of motion corresponding to the values of the auxiliary fields at the lattice sites. Since $\mathcal{Z}_E(t)$ is expressed in terms of $[\det \mathbf{M}(s(\vec{n}, n_t), t)]^2$, the "potential energy" function is given by [38, 53]

$$V(s(\vec{n}, n_t)) = -2 \log(|\det \mathbf{M}(s(\vec{n}, n_t), t_{end})|)\,, \tag{3.11}$$

where $t_{end} \leq L_t$ is the largest Euclidean time at which we measure $\mathcal{Z}_E(t)$. This gives an HMC Hamiltonian of

$$H_{\text{HMC}}(s,p) = \frac{1}{2} \sum_{\vec{n},n_t} \Big(p(\vec{n}, n_t))^2 + V(s)\,, \tag{3.12}$$

where $p(\vec{n}, n_t)$ is the conjugate momentum for $s(\vec{n}, n_t)$. This HMC Hamiltonian corresponds to sampling configurations $s(\vec{n}, n_t)$ according to the probability weight

$$P(s) = \exp\Big(-\frac{1}{2}\sum_{\vec{n},n_t}(p(\vec{n}, n_t))^2 + 2\log(|\det \mathbf{M}(s(\vec{n}, n_t), t_{end})|)\Big) \tag{3.13}$$

This implies that we are sampling according to a weight that is proportional to the integrand in Eq. (2.35):

$$\begin{aligned} P(s) &\propto \exp\Big(2\log(|\det \mathbf{M}(s(\vec{n}, n_t), t_{end})|)\Big) \\ &= \left[\det \mathbf{M}(s(\vec{n}, n_t), t_{end})\right]^2 . \end{aligned} \tag{3.14}$$

3.3.3 HMC Algorithm

The outline of the steps of the HMC algorithm are as follows [30, 39]:

1. Choose a small $\varepsilon_{\text{step}} > 0$ and a natural number N_{step} for the step size and trajectory length, respectively, for use in the discretized Hamilton's equations of motion.
2. Randomly generate an initial auxiliary field configuration $s^0(\vec{n}, n_t)$ according to the Gaussian distribution
$$P(s^0(\vec{n}, n_t)) \propto \exp\Big(-\frac{1}{2}(s^0(\vec{n}, n_t))^2\Big) \tag{3.15}$$
3. Randomly generate a configuration $p^0(\vec{n}, n_t)$ according to the Gaussian distribution
$$P(p^0(\vec{n}, n_t)) \propto \exp\Big(-\frac{1}{2}(p^0(\vec{n}, n_t))^2\Big) \tag{3.16}$$
4. For each $\vec{n}$ and n_t on the space-time lattice, let
$$\tilde{p}^0(\vec{n}, n_t) = p^0(\vec{n}, n_t) - \frac{\varepsilon_{\text{step}}}{2}\frac{\partial V(s)}{\partial s}\Big|_{s=s^0}, \tag{3.17}$$
where $\frac{\partial V(s)}{\partial s}$ is calculated using [38]
$$\begin{aligned} \frac{\partial}{\partial s}\log(\det M) &= \frac{1}{\det M}\frac{\partial}{\partial s}\det M \\ &= \frac{1}{\det M}\sum_{k,l}\frac{\partial M}{\partial M_{kl}}\frac{\partial M_{kl}}{\partial s} \\ &= \sum_{k,l}\left[M^{-1}\right]_{lk}\frac{\partial M_{kl}}{\partial s} . \end{aligned} \tag{3.18}$$

5. For each HMC time step $k = 0, 1, \ldots, N_{\text{step}} - 1$ and each $\vec{n}$ and n_t on the lattice, let

$$s^{k+1}(\vec{n}, n_t) = s^k(\vec{n}, n_t) + \varepsilon_{\text{step}} \tilde{p}^k(\vec{n}, n_t) \tag{3.19}$$

$$\tilde{p}^{k+1}(\vec{n}, n_t) = \tilde{p}^k(\vec{n}, n_t) - \varepsilon_{\text{step}} \frac{\partial V(s)}{\partial s}\Bigg|_{s=s^{k+1}} . \tag{3.20}$$

6. For each $\vec{n}$ and n_t on the lattice, let

$$p^{N_{\text{step}}}(\vec{n}, n_t) = \tilde{p}^{N_{\text{step}}}(\vec{n}, n_t) + \frac{\varepsilon_{\text{step}}}{2} \frac{\partial V(s)}{\partial s}\Bigg|_{s=s^{N_{\text{step}}}} . \tag{3.21}$$

7. Let $r \in [0, 1)$ be chosen from a uniform distribution.
   If $r < \exp(-H_{\text{HMC}}(s^{N_{\text{step}}}, p^{N_{\text{step}}}) + H_{\text{HMC}}(s^0, p^0))$ then put $s^0 = s^{N_{\text{step}}}$.

8. Go back to step 3 to start a new trajectory.

A proposed configuration is always accepted if it has a lower HMC energy than the current configuration. If a proposed configuration has a higher HMC energy than the current configuration then it is accepted with some probability as determined by step 7. This is often referred to as the "Metropolis step," in reference to the aforementioned Metropolis-Hastings algorithm.

Steps 3-7 are repeated for as many configurations as desired. For each configuration we calculate the ratio

$$O(s) = \frac{[\det \mathbf{M}(s, t_{end})]^2}{[\det \mathbf{M}(s, t_{end} - 1)]^2} . \tag{3.22}$$

The ensemble average of $O(s)$ approximates the quantity

$$\frac{\mathcal{Z}_E(t_{end})}{\mathcal{Z}_E(t_{end} - 1)} , \tag{3.23}$$

which gives an estimate for the energy of the system at time t_{end} using Eq. (2.39).

Each HMC simulation is run across many different processors which each follow completely independent trajectories. The ensemble averages and errors are computed using the

results from each processor. The errors obtained from the HMC simulations are statistical in nature, unlike the errors related to finite-volume sizes and non-zero lattice spacings introduced in Chapter 2.

3.3.4 Calculating the Ground State Energies

In order to estimate the ground state energy E_0 of the dimer-dimer system we ran the HMC simulations for various L_t values and performed an exponential decay fit to extrapolate the energy in the $L_t \to \infty$ limit. Fitting the data to the form

$$E(t) = E_0 + d_1 e^{-d_2 t} \tag{3.24}$$

with fit parameters d_1 and d_2 seems reasonable, but excited states often ruin the fit at small L_t.

A much better form can be derived so that it fits more data points over a wider range of L_t values. Consider a wave function $|\psi\rangle$ expanded in an orthonormal set of eigenstates of the Hamiltonian H,

$$|\psi_0\rangle = \sum_n c_n |\phi_n\rangle \ , \tag{3.25}$$

$$\begin{aligned} |\psi_{t/2}\rangle =& e^{-Ht/2} \sum_n c_n |\phi_n\rangle \\ =& \sum_n c_n e^{-E_n t/2} |\phi_n\rangle \ , \end{aligned} \tag{3.26}$$

and then define

$$\begin{aligned} E(t) =& \frac{\langle \psi_{t/2}| H |\psi_{t/2}\rangle}{\langle \psi_{t/2}|\psi_{t/2}\rangle} \\ =& \frac{\sum_n |c_n|^2 E_n e^{-E_n t}}{\sum_n |c_n|^2 e^{-E_n t}} \ . \end{aligned} \tag{3.27}$$

Separately truncating the numerator and denominator yields the desired fit form:

$$E(t) = \frac{E_0 + d_3 E_1 e^{-\Delta_1 t}}{1 + d_3 e^{-\Delta_1 t}}\,, \tag{3.28}$$

where $d_3 = |c_1|^2/|c_0|^2$ and $\Delta_1 = E_1 - E_0$. Notice that for sufficiently small $d_3 e^{-\Delta_1 t}$,

$$\begin{aligned} E(t) \approx & (E_0 + d_3 E_1 e^{-\Delta_1 t})(1 - d_3 e^{-\Delta_1 t}) \\ \approx & E_0 + d_3 \Delta_1 e^{-\Delta_1 t}\,, \end{aligned} \tag{3.29}$$

and so we obtain Eq. (3.24) if we let $d_1 = d_3\Delta_1$ and $d_2 = \Delta_1$.

For comparison, Figure 3.2 shows fits to the same $B^{(\infty)} = 5.0$ MeV and $L = 10$ data set using both Eq. (3.24) and Eq. (3.28). In the figure, these fit forms are denoted by "Model A" and "Model B," respectively. These choices of numerical parameters are discussed in Section 4.1.

3.3.5 HMC Efficiency

The efficiency of the HMC calculations can be dramatically improved by running the simulations in a different way. Rather than starting the simulations with all four fermions interacting, for the first L_t' Euclidean time steps the simulation is run with only one spin-up and one spin-down particle to allow it to construct a dimer. After the L_t' time steps the full system is then run. This technique significantly improves the previous method (which is equivalent to $L_t' = 0$). Figure 3.3[2] shows a comparison of these two methods using lattice data for $B^{(\infty)} = 2.2246$ MeV and $L = 6$.

[2]This figure is taken from Ref. [54].

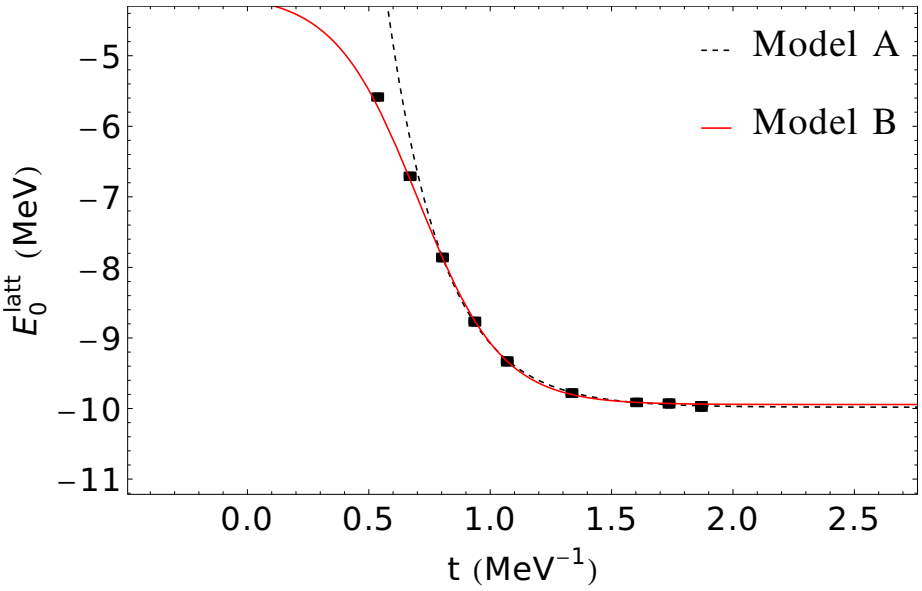

Figure 3.2

Fits for $B^{(\infty)} = 5.0$ MeV and $L = 10$

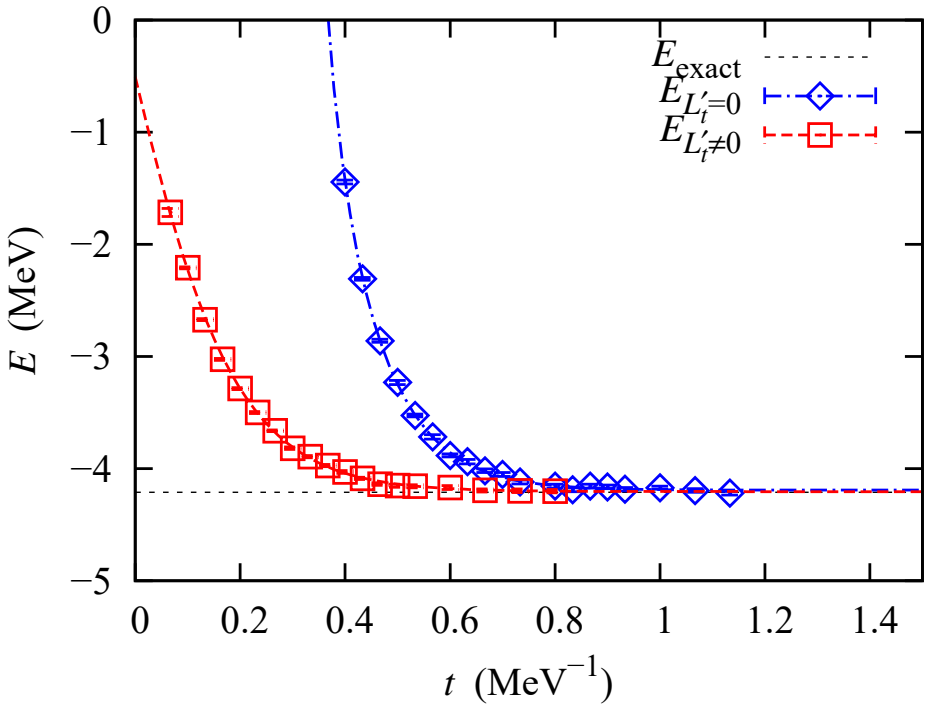

Figure 3.3

Comparison of HMC calculations with $L_t' = 0$ and $L_t' \neq 0$

CHAPTER 4

DATA AND ANALYSIS

4.1 Numerical Parameters

We consider lattice box lengths of $L = 4, 5, 6, 7, 8, 9, 10, 12$ using spatial and temporal lattice spacings of $b = 1/100$ MeV^{-1} and $b_t = 1/150$ MeV^{-1}, respectively. This corresponds to physical box lengths ranging from about 8 fm to 24 fm with a spatial lattice spacing of almost 2 fm.

We consider two-body binding energies of $B^{(\infty)} = 2.2246, 3.0, 3.5, 5.0$ MeV. $B^{(\infty)} = 2.2246$ MeV corresponds to the binding energy of the deuteron. We also take the fermion mass to be $m = 939$ MeV. This corresponds to the approximate masses of the neutron and proton that make up the deuteron. The final results are universal and do not depend on these particular choices of numerical parameters.

For the Hybrid Monte Carlo algorithm parameters discussed in Section 3.3.3, we chose $\varepsilon_{\text{step}} = 0.1$ and $N_{\text{step}} = 10$.

4.2 Data

With our current computational resources, exact matrix calculations were feasible for lattice lengths of $L \leq 6$. Table 4.1 shows a comparison between the energies E_0^{exact} obtained from exact transfer matrix (without auxiliary field) calculations and the energies

E_0^{latt} obtained from lattice HMC simulations for each $L \leq 6$ and for each binding energy $B^{(\infty)}$. This table also shows the topological factors $\tau_{\text{d}}^{(L)}$ which were calculated using the corresponding $B^{(\infty)}$ and E_0^{latt}. As discussed in Section 3.2.3, $\tau_{\text{d}}^{(L)}$ increases as L increases. The lattice HMC data shows good agreement with the exact results, so we expect the results for lattice lengths $L > 6$ to be accurate.

Table 4.1

Comparison between HMC and exact matrix calculations

$B^{(\infty)}$ (MeV)	L	E_0^{latt} (MeV)	E_0^{exact} (MeV)	$\tau_{\text{d}}^{(L)}$
2.2246	4	-3.210 ± 0.006	-3.214	0.3879
2.2246	5	-3.922 ± 0.006	-3.936	0.4579
2.2246	6	-4.200 ± 0.008	-4.212	0.5352
3.0	4	-5.067 ± 0.007	-5.065	0.4223
3.0	5	-5.634 ± 0.005	-5.634	0.5106
3.0	6	-5.823 ± 0.006	-5.827	0.6048
3.5	4	-6.199 ± 0.005	-6.203	0.4419
3.5	5	-6.709 ± 0.013	-6.693	0.5444
3.5	6	-6.845 ± 0.009	-6.848	0.6451
5.0	4	-9.471 ± 0.002	-9.466	0.4991
5.0	5	-9.788 ± 0.004	-9.784	0.6247
5.0	6	-9.863 ± 0.004	-9.868	0.7436

4.2.1 Scatter Plot

Writing the ERE for the dimer-dimer system and truncating terms of higher order than p^4 we obtain

$$p \cot \delta_{\text{dd}}(p) = -\frac{1}{a_{\text{dd}}} + \frac{1}{2} r_{\text{dd}} p^2 + \frac{1}{2} s_{\text{dd}} p^4 \,, \tag{4.1}$$

where $a_{\rm dd}$ is the dimer-dimer scattering length, $r_{\rm dd}$ is the dimer-dimer effective range and $s_{\rm dd}$ is the so-called dimer-dimer shape parameter. By multiplying Eq. (4.1) by the lattice fermion-fermion scattering length $a_{\rm ff}^{\rm latt}$ we obtain

$$(a_{\rm ff}^{\rm latt}p)\cot\delta_{\rm dd}(p) = -\frac{1}{a_0^{\rm latt}} + \frac{1}{2}r_0^{\rm latt}(a_{\rm ff}^{\rm latt}p)^2 + \frac{1}{2}s_0^{\rm latt}(a_{\rm ff}^{\rm latt}p)^4\,, \tag{4.2}$$

where $a_0^{\rm latt} = a_{\rm dd}/a_{\rm ff}^{\rm latt}$, $r_0^{\rm latt} = r_{\rm dd}/a_{\rm ff}^{\rm latt}$ and $s_0^{\rm latt} = s_{\rm dd}/(a_{\rm ff}^{\rm latt})^3$. The presence of $a_{\rm ff}^{\rm latt}$ in Eq. (4.2) makes the equation dimensionless, and it will also be used in extrapolating the continuum values of the dimer-dimer ERE parameters. As discussed in Section 3.2.3, the p and $\delta_{\rm dd}$ can be determined for each ground state energy E_0 found for a particular binding energy $B^{(\infty)}$ and lattice length L.

For each energy E_0, the relative momentum p of the dimer-dimer system is calculated using the iterative procedure described in Section 3.2.3, and then $p\cot\delta_{\rm dd}(p)$ is determined by using this p in Lüscher's formula. Since each E_0 has an associated statistical error ΔE_0 from the HMC simulations, both p and $p\cot\delta_{\rm dd}(p)$ have errors in their values. We use a scatter plot to help take these errors into account.

We begin by taking an odd number of evenly-spaced energies E from within the interval $[E_0 - \Delta E_0, E_0 + \Delta E_0]$. For each E we can calculate p and $p\cot\delta_{\rm dd}(p)$ values and then generate a scatter plot of $(a_{\rm ff}^{\rm latt}p)\cot\delta_{\rm dd}(p)$ vs. $(a_{\rm ff}^{\rm latt}p)^2$. We fit in the low-momentum limit by only using data points with $(a_{\rm ff}p)^2 \lesssim 0.4$.

An example of the scatter plot and fit is shown in Figure 4.1 for $B^{(\infty)} = 5.0$ MeV where the clusters of points correspond to $L = 6, 7, 8, 9$. The solid line is the fitted function

$f(x) = -\frac{1}{a_0^{\text{latt}}} + \frac{1}{2} r_0^{\text{latt}} x + \frac{1}{2} s_0^{\text{latt}} x^2$ with $a_0^{\text{latt}} = 0.709$, $r_0^{\text{latt}} = 4.2$, and $s_0^{\text{latt}} = -6.7$. A complete list of ERE parameters for all binding energies $B^{(\infty)}$ is given in Table 4.2.

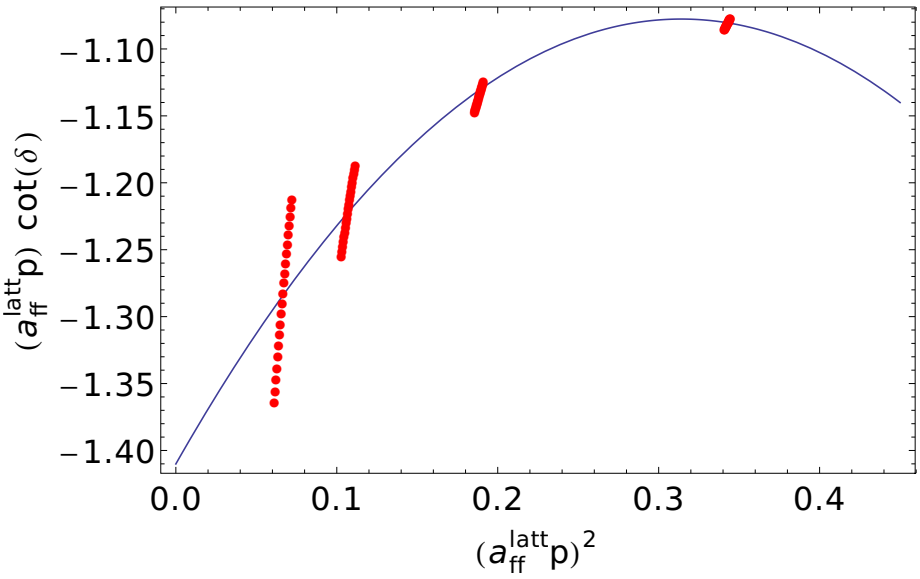

Figure 4.1

Scatter plot for $B^{(\infty)} = 5.0$ MeV with 21 cluster points

As seen in Table 3.1, larger $B^{(\infty)}$ corresponds to smaller $a_{\text{ff}}^{\text{latt}}$. To obtain the continuum values for $a_{\text{dd}}/a_{\text{ff}}$ we fit the data points $(b/a_{\text{ff}}^{\text{latt}}, a_0^{\text{latt}})$ to the form

$$a_0^{\text{latt}} = a_0 + a_1 \frac{b}{a_{\text{ff}}^{\text{latt}}}\,, \tag{4.3}$$

where b is the lattice spacing and a_1 is a miscellaneous fit parameter. Likewise, for the continuum value of $r_{\text{dd}}/a_{\text{ff}}$, we fit the data points $(b/a_{\text{ff}}^{\text{latt}}, r_0^{\text{latt}})$ to the form

$$r_0^{\text{latt}} = r_0 + r_1 \frac{b}{a_{\text{ff}}^{\text{latt}}}\,, \tag{4.4}$$

Table 4.2

Dimer-dimer lattice ERE parameters using scatter plots

$B^{(\infty)}$ (MeV)	$a_0^{\rm latt}$	$r_0^{\rm latt}$	$s_0^{\rm latt}$
2.2246	0.664 ± 0.009	4.0 ± 0.3	-4.7 ± 0.6
3.0	0.691 ± 0.006	3.9 ± 0.2	-5.3 ± 0.4
3.5	0.709 ± 0.008	3.8 ± 0.3	-5.9 ± 0.7
5.0	0.709 ± 0.006	4.2 ± 0.3	-6.7 ± 0.6

where r_1 is a miscellaneous fit parameter. Plots showing the data points and fits are shown in Figure 4.2 and Figure 4.3, respectively.

We use the $b/a_{\rm ff}^{\rm latt} \to 0$ limit in Eq. (4.3) and Eq. (4.4) to extrapolate the continuum values of $a_0 = a_{\rm dd}/a_{\rm ff}$ and $r_0 = r_{\rm dd}/a_{\rm ff}$. These values are given in Table 4.3. Our value for $a_{\rm dd}/a_{\rm ff}$ shows excellent agreement with the previously cited value obtained using exact numerical calculations. Our value for $r_{\rm dd}/a_{\rm ff}$ is positive, which agrees in sign with the previously cited value, although it is larger in magnitude.

In s-wave potential scattering with momentum p and a hard sphere potential of radius $R > 0$, the phase shift $\delta(p) = -pR$ [10]. This yields a positive effective range because $p\cot(-pR) \approx -\frac{1}{R} + \frac{1}{2}(\frac{2R}{3})p^2$ for small p. Our dimer-dimer system is also under the influence of a repulsive interaction due to the Pauli exclusion principle, therefore the $r_{\rm dd}/a_{\rm ff} > 0$ result seems reasonable. Since $a_{\rm ff}$ is the only available scale, it is unclear why it should be the case that $r_{\rm dd}/a_{\rm ff} \ll 1$ as it is for the cited value.

A more sophisticated analysis, which fits the data simultaneously in the momentum p and lattice spacing b directions, is explored in Ref. [54]. This analysis takes into account

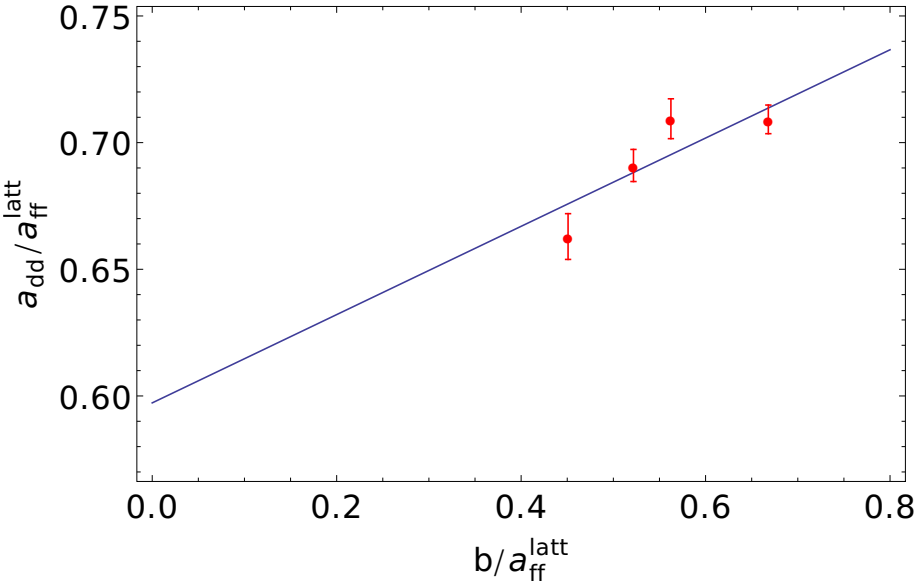

Figure 4.2

Linear fit for $a_{\mathrm{dd}}/a_{\mathrm{ff}}$ using Eq. (4.3)

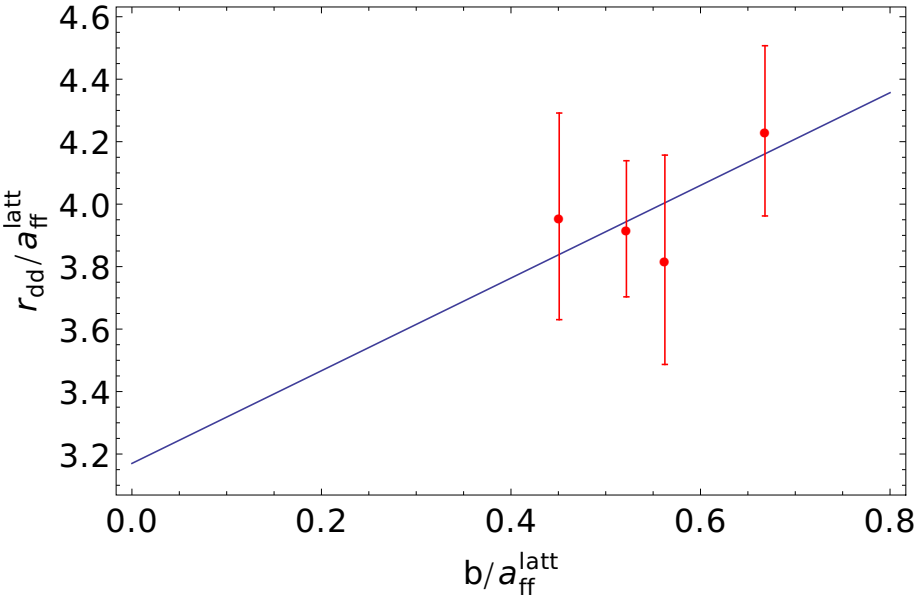

Figure 4.3

Linear fit for $r_{\mathrm{dd}}/a_{\mathrm{ff}}$ using Eq. (4.4)

Table 4.3

Dimer-dimer continuum scattering length and effective range

$a_{\rm dd}/a_{\rm ff}$	$r_{\rm dd}/a_{\rm ff}$
0.60 ± 0.04	3.2 ± 0.5

the errors in p and $p \cot \delta_{\rm dd}(p)$ in a more direct way. Using these techniques we find results similar to those in Table 4.3.

4.2.2 Linear Fit with Errors in Both Coordinates

In Section 4.2.1 we fit our data to the ERE by using a scatter plot to try to account for the correlated errors in both coordinates. In this section we will perform a linear fit using a subset of the same data, this time assuming that the errors in both coordinates are independent. This is done as an additional check of our previous results, and we show that the results obtained in this way are comparable to the results in Section 4.2.1. A description of doing linear fits with errors in both coordinates is given in Refs. [55, 56].

Starting again with Eq. (4.1) and truncating terms to obtain the dimer-dimer shape-independent approximation formula yields

$$p \cot \delta_{\rm dd}(p) = -\frac{1}{a_{\rm dd}} + \frac{1}{2} r_{\rm dd} p^2 \,. \tag{4.5}$$

By multiplying Eq. (4.5) by the lattice fermion-fermion scattering length $a_{\rm ff}^{\rm latt}$ we obtain

$$(a_{\rm ff}^{\rm latt} p) \cot \delta_{\rm dd}(p) = -\frac{1}{a_0^{\rm latt}} + \frac{1}{2} r_0^{\rm latt} x \,, \tag{4.6}$$

where $x = (a_{\rm ff}^{\rm latt} p)^2$, $a_0^{\rm latt} = a_{\rm dd}/a_{\rm ff}^{\rm latt}$, and $r_0^{\rm latt} = r_{\rm dd}/a_{\rm ff}^{\rm latt}$. Now we want fit all of the $(x,\ a_{\rm ff}^{\rm latt} p \cot \delta_{\rm dd})$ data to a single straight line while considering the errors in both coordi-

nates. This is in contrast to the previous fits in which each $B^{(\infty)}$ was treated separately. We conservatively estimate the errors using the spread of scatter plot points used in Section 4.2.1. We fit in the low-momentum limit by only using data points with $x \lesssim 0.2$.

Table 4.4 shows the results of the linear fit. These values are comparable to the values in Table 4.2, which is what we wished to show. Figure 4.4 shows a plot of the data points with errors in both directions and the fitting function using the parameters in Table 4.4.

Table 4.4

Dimer-dimer lattice ERE parameters using a linear fit

a_0^{latt}	r_0^{latt}
0.73 ± 0.03	2.6 ± 0.6

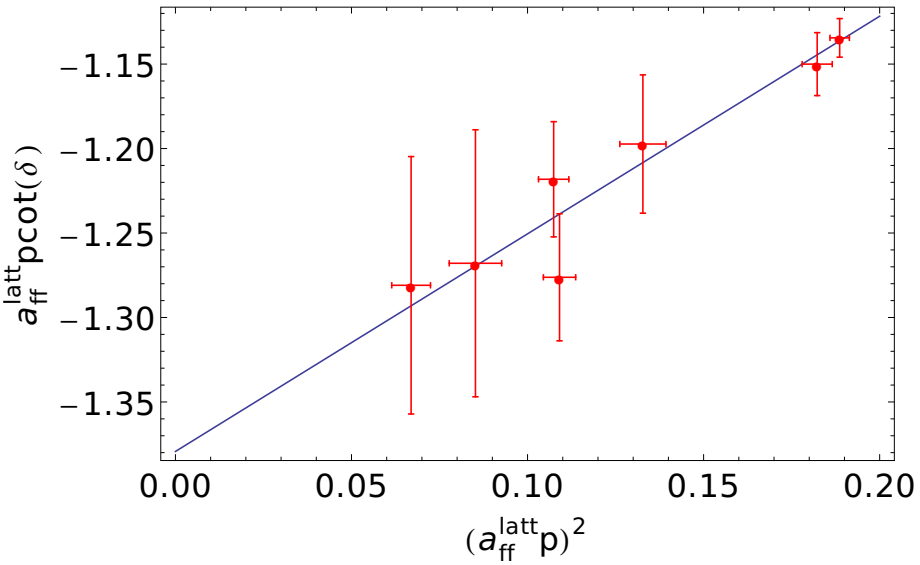

Figure 4.4

Linear fit with errors in both directions shown

CHAPTER 5

CONCLUSIONS

In this work we considered the scattering of a four-body system of non-relativistic spin-1/2 fermions with a two-body contact interaction capable of producing a bound state known as a dimer. We started with a continuum theory which was constructed in the framework of Effective Field Theory. Given that the particles of interest are fermions, this demands that the contact interaction be in the spin (or isospin, where applicable) anti-symmetric channel.

We then introduced the notion of Euclidean Time Projection, which allows us to extract information about the ground state of a system by studying its properties in the limit of large Euclidean time. This, in essence, allowed us to study our four-body system using ideas from thermal physics.

We then proceeded to discretize this continuum theory into a periodic space-time lattice. We eventually rewrote the partition function of the system in terms of an auxiliary field and the square of the determinant of a real matrix. This shows that, unlike many other systems of interacting fermions, there is no "sign problem."

For a variety of continuum fermion-fermion binding energies and lattice sizes, we used Hybrid Monte Carlo methods to calculate the ground state energies of the scattering four-

body system. The ground state of this four-fermion system consists of two dimers, which enabled us to study a two-dimer system. Given the ground state energy, we then calculated the relative momentum of the two dimers. Given this momentum, Lüscher's formula allowed us to find the value of $p \cot \delta_{\mathrm{dd}}(p)$ for the two-dimer system, which in turn allowed us to determine the dimer-dimer scattering length a_{dd} and effective range r_{dd} by using the Effective Range Expansion.

We calculated the ground state energies of the two-dimer system for a variety of lattice volumes up to about $24 \times 24 \times 24\,\mathrm{fm}^3$ and fermion-fermion binding energies up to 5.0 MeV. Our HMC calculations reproduced the exact ground state energies obtained through exact matrix operations for lattice volumes up to about $12 \times 12 \times 12\,\mathrm{fm}^3$. This gives us confidence in the results of this method and we expect the results for larger lattice volumes to be accurate.

Using these techniques we obtained a dimer-dimer scattering length of $a_{\mathrm{dd}}/a_{\mathrm{ff}} = 0.60 \pm 0.04$, which is in good agreement with the cited value obtained through exact numerical calculations, $a_{\mathrm{dd}}/a_{\mathrm{ff}} = 0.60 \pm 0.01$. We also obtained a dimer-dimer effective range of $r_{\mathrm{dd}}/a_{\mathrm{ff}} = 3.2 \pm 0.5$, which agrees in sign, although not in magnitude, with the cited value of $r_{\mathrm{dd}}/a_{\mathrm{ff}} \approx 0.12$.

A different analysis of our data is explored in Ref. [54]. This fits the data in the momentum and lattice spacing directions simultaneously, unlike the scatter plot method used above. We find similar results using both techniques. Further work could also consider running HMC simulations with larger lattice box sizes and better statistics. This would make it possible to use smaller momenta values for the fits.

REFERENCES

[1] R. Newton, *Scattering Theory of Waves and Particles*, 2nd ed. (Dover Publications, Mineola, New York, 2002).

[2] J. Schwinger, *A Variational Principle for Scattering Problems*, Phys. Rev. **72**, 742 (1947).

[3] H. A. Bethe, *Theory of the Effective Range in Nuclear Scattering*, Phys. Rev. **76**, 38 (1949).

[4] H. A. Bethe and C. Longmire, *The Effective Range of Nuclear Forces II. Photo-Disintegration of the Deuteron*, Phys. Rev. **77**, 647 (1950).

[5] H.-W. Hammer and D. Lee, *Causality and the effective range expansion*, Annals Phys. **325**, 2212 (2010).

[6] J. M. Blatt and J. D. Jackson, *On the Interpretation of Neutron-Proton Scattering Data by the Schwinger Variational Method*, Phys. Rev. **76** (1949).

[7] J. R. Taylor, *Scattering Theory: The Quantum Theory of Nonrelativistic Collissions* (Robert E. Krieger Publishing, Malabar, Florida, 1983).

[8] M. L. Goldberger and K. M. Watson, *Collision Theory* (John Wiley & Sons, New York, 1964).

[9] K. Gottfried, *Quantum Mechanics* (W. A. Benjamin, Reading, Massachusetts, 1974).

[10] J. J. Sakurai, *Modern Quantum Mechanics* (Addison-Wesley Longman, New York, 1994).

[11] Q. Chen *et al.*, *Measurement of the neutron-neutron scattering length using the pi-d capture reaction*, Phys. Rev. C **77**, 054002 (2008).

[12] J. Deng, A. Siepe and W. von Witsch, *New measurement of the neutron-proton scattering length a_{np} via the n-d breakup reaction at 25 MeV*, Phys. Rev. C **66**, 047001 (2002).

[13] K. Schoen *et al.*, *Precision neutron interferometric measurements and updated evaluations of the n-p and n-d coherent neutron scattering lengths*, Phys. Rev. C **67**, 044005 (2003).

[14] S. Giorgini, L. P. Pitaevskii and S. Stringari, *Theory of Ultracold Atomic Fermi Gases*, Rev. Mod. Phys. **80**, 1215 (2008).

[15] K. M. O'Hara, S. L. Hemmer, M. E. Gehm, S. R. Granade and J. E. Thomas, *Observation of a Strongly Interacting Degenerate Fermi Gas of Atoms*, Science **13**, 2179 (2002).

[16] C. A. Regal, M. Greiner and D. S. Jin, *Observation of Resonance Condensation of Fermionic Atom Pairs*, Phys. Rev. Lett. **92**, 040403 (2004).

[17] D. S. Petrov, C. Salomon and G. V. Shlyapnikov, *Weakly Bound Dimers of Fermionic Atoms*, Phys. Rev. Lett. **93**, 090404 (2004).

[18] D. S. Petrov, C. Salomon and G. V. Shlyapnikov, *Scattering properties of weakly bound dimers of fermionic atoms*, Phys. Rev. A **71**, 012708 (2005).

[19] G. Rupak, *Dimer scattering in the ε expansion*, nucl-th/0605074.

[20] J. P. D'Incao, S. T. Rittenhouse, N. P. Mehta and C. H. Greene, *Dimer-dimer collisions at finite energies in two-component Fermi gases*, Phys. Rev. A **79**, 030501 (2009).

[21] J. von Stecher, C. H. Greene and D. Blume, *BEC-BCS crossover of a trapped two-component Fermi gas with unequal masses*, Phys. Rev. A **76**, 053613 (2007).

[22] J.-W. Chen, G. Rupak and M. J. Savage, *Nucleon-nucleon effective field theory without pions*, Nucl. Phys. A **653**, 386 (1999).

[23] P. F. Bedaque and U. van Kolck, *Effective Field Theory for Few-nucleon Systems*, Ann. Rev. Nucl. Part. Sci. **52**, 339 (2002).

[24] M. Peskin and D. Schroeder, *An Introduction to Quantum Field Theory* (Westview Press, Boulder, Colorado, 1995).

[25] O. A. Yakubovski, *On the Integral equations in the theory of N particle scattering*, Sov. J. Nucl. Phys. **5**, 937 (1967).

[26] F. Ciesielski and J. Carbonell, *Solutions of the Faddeev-Yakubovsky equations for the four nucleon scattering states*, Phys. Rev. C **58**, 58 (1998).

[27] A. K. Motovilov, *Progress in methods to solve the Faddeev and Yakubovsky differential equations*, Few-Body Systems **43**, 121 (2008).

[28] G. C. Wick, *Properties of Bethe-Salpeter Wave Functions*, Phys. Rev. **96**, 1124 (1954).

[29] E. Epelbaum, H. Krebs, T. Lähde, D. Lee and U.-G. Meißner, *Structure and rotations of the Hoyle state*, Phys. Rev. Lett. **109**, 252501 (2012).

[30] D. Lee, *Ground state energy at unitarity*, Phys. Rev. C **78**, 024001 (2008).

[31] J. Hubbard, *Calculation of Partition Functions*, Phys. Rev. Lett. **3**, 77 (1959).

[32] R. L. Stratonovich, *On a Method of Calculating Quantum Distribution Functions*, Sov. Phys. Doklady **2**, 416 (1958).

[33] M. Creutz, *Transfer matrices and lattice fermions at finite density*, Found. Phys. **30**, 487 (2000).

[34] D. Lee, *Superfluidity and excitations at unitarity*, Phys. rev. B **75**, 134502 (2007).

[35] J. E. Y. Loh *et al.*, *Sign problem in the numerical simulation of many-electron systems*, Phys. Rev. B **41**, 9301 (1990).

[36] M. Troyer and U.-J. Wiese, *Computational Complexity and Fundamental Limitations to Fermionic Quantum Monte Carlo Simulations*, Phys. Rev. Lett. **94**, 170201 (2005).

[37] D. Lee and T. Schäfer, *Neutron matter on the lattice with pionless effective field theory*, Phys. Rev. C **72**, 024006 (2005).

[38] D. Lee, *Ground-state energy of spin-1/2 fermions in the unitary limit*, Phys. rev. B **73**, 115112 (2006).

[39] D. Lee, *Lattice simulations for few- and many-body systems*, Prog. Part. Nucl. Phys. **63**, 117 (2009).

[40] M. Lüscher, *Volume dependence of the energy spectrum in massive quantum field theories: 1. stable particle states*, Commun. Math. Phys. **104**, 177 (1986).

[41] M. Lüscher, *Volume dependence of the energy spectrum in massive quantum field theories: 2. scattering states*, Commun. Math. Phys. **105**, 153 (1986).

[42] M. Lüscher, *Two particle states on a torus and their relation to the scattering matrix*, Nucl. Phys. B **354**, 531 (1991).

[43] S. Koenig, D. Lee and H.-W. Hammer, *Volume Dependence of Bound States with Angular Momentum*, Phys. Rev. Lett. **107**, 112001 (2011).

[44] S. Koenig, D. Lee and H.-W. Hammer, *Non-relativistic bound states in a finite volume*, Annals Phys. **327**, 1450 (2012).

[45] S. Bour, H.-W. Hammer, D. Lee and U.-G. Meißner, *Benchmark calculations for elastic fermion-dimer scattering*, Phys. Rev. C **86**, 034003 (2012).

[46] Y. A. Rozanov, *Probability Theory: A Concise Course* (Dover Publications, Mineola, New York, 1977).

[47] B. A. Berg, *Markov Chain Monte Carlo Simulations and Their Statistical Analysis* (World Scientific Publishing, Singapore, 2006).

[48] J. M. Thijssen, *Computational Physics*, 2nd ed. (Cambridge University Press, New York, 2007).

[49] D. P. Landau and K. Binder, *A Guide to Monte Carlo Simulations in Statistical Physics* (Cambridge University Press, Cambridge, United Kingdom, 2000).

[50] J. M. Hammersley and D. C. Handscomb, *Monte Carlo Methods* (Spottiswoode, Ballantyne & Co., Great Britain, 1964).

[51] N. Metropolis, A. W. Rosenbluth, M. N. Rosenbluth, A. H. Teller and E. Teller, *Equation of State Calculations by Fast Computing Machines*, J. Chem. Phys. **21**, 1087 (1953).

[52] W. K. Hastings, *Monte Carlo Sampling Methods Using Markov Chains and Their Applications*, Biometrika **57**, 97 (1970).

[53] R. M. Neal, MCMC Using Hamiltonian Dynamics, in *Handbook of Markov Chain Monte Carlo*, pp. 113–162, Chapman & Hall/CRC, 2011.

[54] S. Elhatisari, K. Katterjohn, D. Lee and G. Rupak, *Dimer-dimer scattering in lattice effective field theory*, In publication.

[55] B. C. Reed, *Linear least-squares fits with errors in both coordinates*, Am. J. Phys. **57**, 642 (1989).

[56] B. C. Reed, *Linear least-squares fits with errors in both coordinates. II. Comments on parameter variances*, Am. J. Phys. **60**, 59 (1992).